# Enhanced understanding of dominant drivers of Water Yield change across China through the improved coupled carbon and water model

Huilan Shen [1, 2], Hanbo Yang [1, 2, *], Changming Li [1,2,3]

[1] Department of Hydraulic Engineering, Tsinghua University, Beijing 100084, China

[2] State Key Laboratory of Hydroscience and Engineering, Tsinghua University, Beijing 100084, China

[3] School of Civil Engineering and Transportation, State Key Laboratory of Subtropical Building and Urban Science, South China University of Technology, Guangzhou 510641, China

* Correspondence: Hanbo Yang (yanghanbo@tsinghua.edu.cn)

**Abstract:** The rapid environmental changes, including climate change, escalating atmospheric $CO_2$ concentration ([$CO_2$]), and vegetation dynamics, have been significantly impacting hydrological processes. Yet disentangling the respective contributions of climate, vegetation, and [CO2] change to water yield (WY)—especially clarifying [CO2]-driven physiological effects—remains difficult. Therefore, this study improved the coupled carbon and water (CCW) model by integrating dynamic water-use efficiency (WUE) to better capture [$CO_2$] physiological feedbacks. Using scenario analysis, WY changes across China from 1982 to 2017 were attributed to climate, vegetation, and [$CO_2$] drivers. The results showed that climate change (especially precipitation change) emerged as the dominant driver, directly affecting over 70% of China's land area. The vegetation change was the second largest factor to reduce WY, especially in central China. The effect of the escalating [$CO_2$] was relatively small. Spatial analysis aligned with isohyetal lines further revealed that vegetation change and [$CO_2$] exerted greater influence within the 400–1600 mm precipitation range. In addition, the elasticity analysis showed that the sensitivity ranking of impact factors is precipitation > [$CO_2$] > NDVI for the whole China. Therefore, CMIP6 SSP585 projections indicate that accelerating [$CO_2$] rise will amplify its hydrological effect to a +1.29% annual WY increase by 2100, surpassing vegetation influences, implying a stronger hydrological role under future forcing. By explicitly representing dynamic WUE, this study improves process-based WY attribution and shows that [$CO_2$] physiological regulation can partly offset vegetation-induced WY reductions, thereby providing new insights for regional water resource management under climate change.

**Keywords:** the coupled carbon and water (CCW) model; WY change; climate change; vegetation change; increasing atmospheric $CO_2$ concentrations; attribution analysis

**Plain language:** Climate change, rising $CO_2$, and vegetation dynamics are reshaping global water cycle, but their impacts remain unclear. We improved the coupled carbon and water model to analyze China’s water yield changes (1982–2017). Our results

showed that climate change was the dominant driver nationally, vegetation/ $CO_2$ most affected in 400-1600 mm precipitation zones. Projections indicate $CO_2$ may increase WY 1.3% annually by 2100, surpassing other drivers. This work informs sustainable water management.

# 1 Introduction

The global environment has been undergoing rapid changes, impacting hydrological processes through climate change, escalating atmospheric $CO_2$ concentration [$CO_2$], and vegetation dynamics (Piao et al., 2007; Wei et al., 2024). Notably, China has experienced a visible greening trend in recent decades, prompting a heightened focus on ecological and water resource concerns (Chen et al., 2019). Investigating the influence of vegetation changes on runoff has thus emerged as a pivotal research area, aligning with China's increasing emphasis on environmental sustainability. Among hydrological metrics, water yield (WY) is especially relevant because it directly represents the amount of water remaining after evapotranspiration and is therefore closely linked to runoff generation and regional water availability. China's diverse climatic zones and pronounced greening make it an ideal natural laboratory for investigating these ecohydrological feedbacks, with implications for both China (Ogutu et al., 2021; Yang et al., 2019) and other semi-arid and monsoon-influenced regions such as the Sahel, South Asia, and the Mediterranean Basin (Nkiaka et al., 2025; Rahman et al., 2025; Serrano-Notivoli et al., 2022). Understanding how vegetation dynamics, climate change, and [$CO_2$] interact to regulate WY is therefore of both scientific and practical importance for water resource management and ecological restoration under accelerating environmental change.

Several methods have been employed to separate the effects of climate, vegetation, and [$CO_2$] change on runoff change, including paired catchment experiments, statistical methods, and modeling approaches (Zeng et al., 2020). Given that annual water yield (WY) equates to runoff through negligible soil water storage changes, these methodological evaluations directly inform WY attribution frameworks (Zhang et al., 2022b). The paired catchment experiment method, though classical, is limited to small-scale watersheds and is less applicable to larger regions (Peng et al., 2016). Statistical methods, while helpful in identifying correlations, lack a physical basis and are insufficient for explaining the underlying mechanisms of runoff changes (Chen et al.,

2022). Modeling approaches for attribution fall into two broad classes: (i) process-based models that explicitly simulate coupled water–energy–carbon processes, and (ii) conceptual models that approximate these processes with parsimonious, physically interpretable relationships (Zhai and Tao, 2021). Process-based models can capture detailed mechanisms, but they require extensive inputs and many parameters, are sensitive to calibration and equifinality, and are computationally demanding—limitations that hinder basin-to-continental applications over long periods(Jiao et al., 2017; Ma et al., 2023). By contrast, conceptual models retain key ecohydrological mechanisms with far fewer parameters, scale well to large regions, and thus are well suited for large-scale attribution while preserving physical interpretability. Among these conceptual models, the Budyko framework, widely used to separate climate change effects on runoff, quantifies water balance through the aridity index (PET/precipitation) and incorporates a catchment-specific Budyko parameter (n) representing integrated land surface characteristics (e.g., vegetation, soil, topography) (Zhang et al., 2022a, 2016a). However, most Budyko-based applications primarily emphasize climate-driven attribution; vegetation and [$CO_2$] influences are typically introduced only indirectly—by assigning temporal changes in the Budyko parameter (n) to vegetation(Tan et al., 2024; Xue et al., 2022; Zhou et al., 2023) or correlating the Budyko parameter (n) with NDVI (Liu et al., 2024; Tan et al., 2023), and by embedding [$CO_2$] effects through PET adjustments(Liu et al., 2024). These practices conflate vegetation with other controls captured by the Budyko parameter (n) (e.g., soil, topography) and mix [$CO_2$]-physiological impacts with meteorological drivers in PET, making it difficult to isolate vegetation structural change from [$CO_2$]-induced stomatal adjustments and to ascribe mechanisms robustly (Gan et al., 2021).

Specifically, elevated [$CO_2$] reduces stomatal conductance—due to smaller stomatal apertures and increased leaf resistance (Lammertsma et al., 2011; Xu et al., 2016) which decreases transpiration fluxes (ET). At the same time, carbon assimilation rate (GPP) may increase with higher [$CO_2$] availability, but this increase is often less

proportional to the reduction in water loss (Montibeller et al., 2022) The resulting imbalance—lower water loss relative to carbon gain—thus leads to higher water-use efficiency (WUE = GPP / ET). In particular, conventional frameworks that neglect [$CO_2$]-driven physiological feedbacks fail to represent the enhanced water-use efficiency (WUE) of vegetation under elevated [$CO_2$] conditions. This omission leads to ambiguous attribution of runoff variations, as part of the reduction in evapotranspiration induced by stomatal closure is often misinterpreted as a vegetation structural effect rather than a [$CO_2$]-induced physiological adjustment. Although numerous studies have examined vegetation and climate controls on runoff, few have explicitly incorporated the [$CO_2$]–WUE feedback within a mechanistic framework. Most existing approaches either completely ignore this feedback or treat it as a simple empirical or linear relationship, rather than capturing its process-based influence on hydrological responses.

The coupled carbon and water (CCW) model integrates hydrological and ecological processes by mechanistically linking vegetation dynamics to water and carbon fluxes through remote sensing-driven parameterization (Li et al., 2024b; Zhang et al., 2021b, 2022b). Unlike the Budyko framework's empirical parameter "n"—which conflates vegetation effects with unaccounted catchment characteristics—the CCW model links vegetation and hydrology through a single mechanistic chain. In this framework, vegetation structure (NDVI/LAI) determines canopy absorption of photosynthetically active radiation (FPAR) and hence gross primary production (GPP) via light-use efficiency, while evapotranspiration (ET) is coupled to GPP through a biome-specific underlying water-use efficiency (UWUE) term with vapor pressure deficit (VPD) regulation. Nevertheless, the original CCW model, while robust in capturing vegetation-climate interactions, adopts a static UWUE and does not account for $CO_2$-induced physiological changes, specifically long-term enhancements in water-use efficiency (WUE) resulting from elevated [$CO_2$], thereby limiting its capacity to

isolate [$CO_2$] fertilization effects from vegetation structural and climatic influences (Adams et al., 2020; Li et al., 2023).

To address this limitation, our study enhanced the CCW framework by incorporating dynamic WUE responses to [$CO_2$], allowing explicit attribution of runoff changes to three distinct drivers—climate change (eg. precipitation, temperature, and so on), vegetation structural change (NDVI, and land use and land cover (LULC)), and [$CO_2$]-physiological effects (stomatal optimization). This extension advances beyond empirical or regression-based attribution, clarifies how [$CO_2$] modulates vegetation–hydrology interactions across large spatial scales, and provides policy-relevant evidence for sustainable water resource management and ecological restoration in China under accelerating environmental change. .

# 2 Methods and Data

## 2.1 Data sources and processing

Four main datasets were employed in the improved CCW model: vegetation data (NDVI), climate data (precipitation, temperature, shortwave radiation, vapor pressure deficit, and atmospheric pressure), land use and land cover (LULC), and [$CO_2$]. The monthly NDVI dataset used in this study (Table 1) was derived from a daily 0.05° gap-free NDVI dataset in China (https://doi.org/10.6084/m9.figshare.c.7002225.v1) (Li et al., 2024a), which was developed from the NOAA's daily NDVI dataset, applying effective data recognition and spatiotemporal gap-filling techniques. The dataset spans 1981–2023 and provides a spatial resolution of 0.05°, and we used bilinear interpolation to generate the dataset with a spatial resolution of 0.1°.

Climate data (Table 1), including precipitation, air temperature, surface downward shortwave radiation, relative humidity, and atmospheric pressure, were sourced from the China Meteorological Forcing Dataset (CMFD) at the National Tibetan Plateau Data Center (TPDC) of the Institute of Tibetan Plateau Research, Chinese Academy of Sciences (He et al., 2020). The dataset spans 1979–2018 and provides a spatial

resolution of 0.1° and temporal resolutions at 3-hour, daily, monthly, and annual scales. As the dataset did not provide vapor pressure deficit (VPD), we calculated VPD using the method from Howell and Dusek (1995), based on atmospheric pressure, temperature, and relative humidity.

LULC data (Table 1) were obtained from the Zhang et al. (2024) global dataset, which provides consistent multi-temporal global LULC maps at 30 m spatial resolution for 1985–2022. The dataset includes 35 fine-resolution LULC types. For the purposes of this study, and to facilitate LULC change analysis, we merged these 35 LULC types into 17 types using the IGBP classification, based on the method by Yang et al. (2017). Four primary LULC types—cropland, forest, grassland, and bare land—were determined following the method described by Mu et al. (2013). The data were resampled to the 0.1° spatial resolution, ensuring compatibility for modeling within the modified CCW framework.

[$CO_2$] data were sourced from the Mauna Loa Observatory (MLO), Hawaii (20°N, 156°W) (http://cdiac.esd.ornl.gov/ftp/trends/co2/ maunaloa.co2), with yearly observations used to represent national [$CO_2$] levels due to the minimal spatial variation in [$CO_2$] across China (Table 1). These datasets were then used to drive the improved CCW model.

In this study, the hydrological data for model validation from 145 hydrological stations (Fig. 1), each with at least 15 years of continuous data since 1982, was collected from the Hydrological Bureau of the Ministry of Water Resources of China (https://www.mwr.gov.cn/english/). Annual runoff data were calculated from the daily runoff and the catchment area controlled by each hydrological station.

**Table 1**. Hydrology, climate, and vegetation data for the improved CCW model

| Dataset | Original Resolution (spatial/temporal) | Period | Reference |
|---|---|---|---|
| **NDVI** | 0.05° ×0.05° (daily) | 1981 - 2023 | (Li et al., 2024a) |
| **Landcover** | 30m×30m (5-year) | 1985 - 2022 | (Zhang et al., 2024) |
| **Climate** | 0.1° ×0.1° (monthly) | 1979 - 2018 | (He et al., 2020) |

| | | | |
|---|---|---|---|
| **[$CO_2$]** | yearly | 1959 - 2023 | Mauna Loa Observatory, Hawaii |
| **Streamflow** | daily | 1982 - 1995 (or later) | On-site streamflow records and the regional flow summary reports of government |

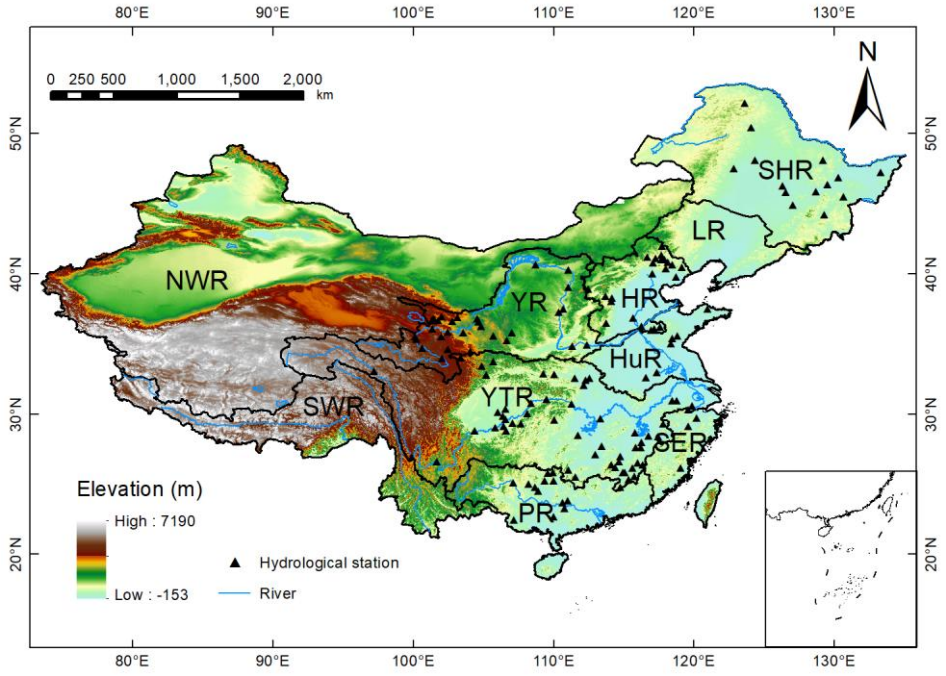


**Figure 1.** The geographic location and topography of the study area, where the black triangles mark the location of the hydrological gauging stations for model evaluation. Ten river basins considered in this study are: Songhua River basin (SHR), Liao River basin (LR), Hai River basin (HR), Huai River basin (HuR), Yangtze River basin (YZR), Yellow River basin (YR), Pearl River basin (PR), Southeast Rivers (SER), Southwest Rivers (SWR) and Northwest Rivers (NWR).

## 2.2 The improved CCW model

The original Coupled Carbon and Water (CCW) model (Zhang et al., 2016b) is a data-driven, remote sensing-based model that effectively integrates carbon and water dynamics to estimate monthly gross primary productivity (GPP) and evapotranspiration (ET). This model, which is particularly carbon-centric, derives ET from GPP constrained by underlying water-use efficiency (UWUE) parameters, which were calibrated using global FLUXNET data (Zhang et al., 2016b; Zhou et al., 2014). Despite its simpler structure, the CCW model achieves accuracy comparable to more complex process-based models in ET estimation. The essential components of the CCW model are represented as:

$$GPP = APAR \times \varepsilon = PAR \times FPAR \times \varepsilon_{pot} \times R_s \times T_s \times W_s \quad (1)$$

where APAR is the absorbed photosynthetically active radiation (MJ $m^{-2}$), which is calculated as the product of incident photosynthetically active radiation (PAR) and the fraction of PAR absorbed by vegetation (FPAR), and PAR is typically assumed to be 45% of the total shortwave radiation (Running et al., 2000); FPAR is determined by the normalized difference vegetation index (NDVI) (Sims et al., 2005); $\varepsilon$ is the realized light-use efficiency (g C $MJ^{-1}$), which is calculated by multiplying the potential light-use efficiency ($\varepsilon_{pot}$) and environmental scalars for diffuse radiation (Rs), temperature (Ts), and moisture stress (Ws). This formulation ensures that GPP estimates reflect the influence of radiation, temperature, and moisture limitations on photosynthetic activity.

In this study, we improve the CCW model by incorporating dynamic water use efficiency (WUE) instead of static UWUE. This enhancement addresses the limitations of the original model, particularly its inability to adapt to environmental changes such as varying [$CO_2$] and vapor pressure deficit (VPD). WUE's estimation method is estimated using the WEC (Water Efficiency and Carbon) equation proposed by Cheng et al. (2017), where WUE is defined at the ecosystem scale as the ratio of GPP to total ecosystem evapotranspiration rather than as a leaf-level intrinsic WUE. Under this framework, evapotranspiration includes transpiration, soil evaporation, and canopy interception, and the analytical upscaling from stomatal theory to ecosystem WUE is represented through the transpiration–soil evaporation partitioning term and the interception term. The final formula for calculating WUE is:

$$WUE = \frac{C_a \times P_a}{1.6\left(VPD + g_1\sqrt{VPD}\right)}[1 - exp(-k * LAI)](1 - f_i) \quad (2)$$

where $C_a$ is atmospheric $CO_2$ concentration (mol($CO_2$) $mol^{-1}$(air)); Pa is atmospheric pressure (kPa); VPD is vapor pressure deficit (kPa); $g_1$ is an empirical parameter of the Ball stomatal conductance model; k is the radiation extinction coefficient, typically set at 0.6, describing how light is absorbed by the canopy; LAI is the leaf area index; and $f_i$ is a factor representing nonproductive water use (such as evaporation from soil and

canopy interception). This equation provides a dynamic estimate of WUE, considering the effects of environmental factors like VPD, $CO_2$ concentration, atmospheric pressure, and canopy structure (LAI). The factor $1-\exp(-k\times LAI)$ represents the partitioning between transpiration and soil evaporation associated with canopy cover at monthly-to-annual scales. In this study, the interception evaporation factor ($f_i$) was set to zero to reduce data requirements and maintain consistency in long-term grid-scale attribution.. This simplification follows previous large-scale ecohydrological studies (Cheng et al., 2017), which reported that canopy interception and soil surface evaporation account for a minor portion of total evapotranspiration at annual to multi-decadal scales. Given that the improved CCW model focused on yearly water yield (WY) dynamics rather than event-scale hydrological responses, neglecting interception loss reduces model complexity without substantially affecting WY estimation.

In order to ensure the consistency of NDVI and LAI trends, we calculated LAI using NDVI (Gutman and Ignatov, 1998) instead of LAI dataset:

$$\begin{cases} LAI = -2ln(1 - f_{NDVI}) \\ f_{NDVI} = \dfrac{NDVI - NDVI_0}{NDVI_1 - NDVI_0} \end{cases} \quad (3)$$

where $NDVI_0 = 0.04$, $NDVI_1 = 0.52$

Evapotranspiration (ET) is then calculated as the ratio of GPP to WUE:

$$ET = \frac{GPP}{WUE} \quad (4)$$

Under this framework, ET should be interpreted as an effective annual ecosystem-scale evapotranspiration suitable for long-term WY attribution, rather than a detailed partitioning of individual ET components. This modification allows the model to estimate ET using dynamic WUE, replacing the static UWUE from the original model. The dynamic nature of WUE enhances the model's ability to simulate ecosystem water use across different environmental conditions and vegetation types.

Finally, the water yield (WY) is calculated as the difference between precipitation (P) and ET:

$$WY = P - ET \quad (5)$$

On an annual scale, WY is assumed to be approximately equal to runoff, as changes in soil water storage over long periods (one year or longer) are considered negligible (Xiao et al., 2020; Zhang et al., 2021b). Thus, the attribution of WY can also be considered as the attribution of runoff. Accordingly, in this study WY is used as the modelled output, while the term 'runoff' is reserved for observed streamflow or literature values explicitly labelled as such. This approximation is most suitable for annual to multi-year analyses in regions without substantial long-term groundwater depletion or strong reservoir regulation.

## 2.3 Attribution analysis framework

To explore the combined and individual effects of climate, vegetation, and [$CO_2$] change on water yield (WY), four scenarios were designed based on data from 1982 to 2017 (Table 2). Scenario 1 (Actual) aimed to validate the improved CCW model and estimate the combined effects of climate, vegetation, and [$CO_2$] change on WY by allowing all variables to vary from 1982 to 2017. Scenario 2 (Vegetation Change) focused on estimating the direct effects of vegetation change on WY by allowing vegetation variables (NDVI and LULC) to vary while keeping climate and [$CO_2$] fixed at 1982 levels. In this case, the trend in WY obtained reflects the impact of vegetation change alone. Scenario 3 (Climate Change) aimed to estimate the direct effects of climate change on WY by allowing climate variables (precipitation, temperature, relative humidity, solar radiation, and atmospheric pressure) to change, while fixing vegetation and [$CO_2$] at 1982 levels. This scenario helps isolate the effects of climate change on WY. Scenario 4 ([$CO_2$] Change) was designed to estimate the direct effects of [$CO_2$] change on WY by varying [$CO_2$] levels from 1982 to 2017, while climate and vegetation variables were fixed at 1982 levels. The resulting WY trend reflects the

impact of [$CO_2$] change alone. The resulting WY series under each scenario represents the direct impact of the corresponding driver under the assumption that the other drivers are fixed.

**Table 2**. Scenario designs in the improved CCW model for WY attribution. LULC: Land use and land cover types; NDVI: Normalized difference vegetation index; TMP: Temperature; SRAD: Shortwave radiation; VPD: Vapor pressure deficit.

| Scenarios | Vegetation | | Climate | | | | | $CO_2$ | Purposes |
|---|---|---|---|---|---|---|---|---|---|
| | LULC | NDVI | P | T | RH | Srad | Pa | $CO_2$ | |
| S1 (baseline) | ▲ | ▲ | ▲ | ▲ | ▲ | ▲ | ▲ | ▲ | Validating the improved CCW model and estimating the combined effects of climate, vegetation, and $CO_2$ change. |
| S2 (vegetation) | ▲ | ▲ | △ | △ | △ | △ | △ | △ | Estimating the direct effects of vegetation change. |
| S3 (climate) | △ | △ | ▲ | ▲ | ▲ | ▲ | ▲ | △ | Estimating the direct effects of climate change. |
| S4 ($CO_2$) | △ | △ | △ | △ | △ | △ | △ | ▲ | Estimating the direct effects of $CO_2$ change. |

Note: The symbol "▲" denotes a changing input variable over time, whereas the symbol "△" represents a fixed input variable at the level of the initial year (1982).

For each scenario, the long-term trend in annual WY over 1982–2017 was quantified using the Theil–Sen estimator, yielding a robust slope. Here, "trend" refers to the Theil–Sen slope of the annual WY series, representing the long-term monotonic rate of change in WY over the study period. The relative contributions of climate, vegetation, and [$CO_2$] to changes in WY were calculated using the following formula (Ma et al., 2023; Wang et al., 2022):

$$\begin{cases} RC_{vegetation} = \dfrac{trend_{vegetation}}{|trend_{vegetation}| + |trend_{climate}| + |trend_{CO2}|} \times 100\% \\ RC_{climate} = \dfrac{trend_{climate}}{|trend_{vegetation}| + |trend_{climate}| + |trend_{CO2}|} \times 100\% \\ RC_{CO2} = \dfrac{trend_{CO2}}{|trend_{vegetation}| + |trend_{climate}| + |trend_{CO2}|} \times 100\% \end{cases} \quad (6)$$

where $trend_{vegetation}$, $trend_{climate}$, and $trend_{CO2}$ denote the Theil–Sen slopes of the annual WY series under vegetation, climate, and [$CO_2$] scenarios, respectively. These slopes represent the long-term rates of WY change attributable to each driver within the scenario framework; the relative contributions ($RC_{vegetation}$, $RC_{climate}$, and $RC_{CO2}$) are expressed as percentages, indicating the normalized magnitude of the scenario-derived direct effects.

At each grid point, the absolute values of the relative contributions of each factor (vegetation, climate, and [$CO_2$]) are compared. For each grid point, we identify the most significant contributor to water yield (WY) changes by comparing the relative contributions of each factor. If the absolute values of the relative contributions of two factors do not exceed 5%, then these two factors are considered joint significant contributors to the changes in WY at that grid point (Jia et al., 2022). This approach helps to highlight areas where the impacts of multiple factors are closely intertwined and both play a critical role in influencing water yield, suggesting that their combined effects are comparable in magnitude. In these cases, the relative contribution of each factor is not significantly stronger than the other, indicating that their combined influence on WY is equally important at the local scale.

The scenario analysis previously conducted revealed the relative contributions of climate, vegetation, and [$CO_2$] to WY changes. However, these contributions arise from both the intrinsic rate of change of each factor and the sensitivity of runoff to those changes (the elasticity coefficient) (Yang and Yang, 2011). To gain a deeper understanding of the changes in WY, we employ elasticity coefficients to quantify its sensitivity to individual factor. We specifically focused on precipitation because,

despite not always having the highest sensitivity, it is integral to the hydrological cycle and essential for assessing water yield (WY) under various climate change scenarios (Liu et al., 2017). The elasticity of runoff refers to the variation in runoff depth resulting from a 1% increase in each climatic variable (Xu et al., 2014). The absolute value of elasticity reflects the sensitivity of runoff to various influencing factors. In other methods, elasticity coefficients are typically calculated using an analytical expression based on instantaneous changes in runoff corresponding to variations in a given factor in a specific year (Fu et al., 2023; Liu et al., 2017; Yang and Yang, 2012). However, in our study, we applied scenario-based analysis over the period of 1982 to 2017. This extended temporal window allowed us to better account for the long-term effects and interactions of multiple factors influencing WY. So we vary each factor (precipitation, NDVI, and [$CO_2$]) by 1% relative to the baseline scenario S1 across the entire 1982-2017 period. We then calculated the annual average runoff values from the adjusted sequence and compared them with the average original baseline runoff values. The difference between these two values, divided by the average baseline runoff value, gave us the runoff change rate:

$$\frac{\Delta R_x}{R_x} = \frac{WY_{mean_x} - WY_{mean_x}}{WY_{mean_x}} \tag{7}$$

Mathematically, the elasticity coefficient is defined as the runoff change rate divided by 1%, and the formula is as follows:

$$\varepsilon_x = \frac{\frac{\Delta R_x}{R_x}}{\frac{\Delta x}{x}} = \frac{\frac{\Delta R_x}{R_x}}{1\%} \tag{8}$$

Generally, while the scenario analysis above has identified which factors are most influential based on their relative contributions, the elasticity coefficients allow us to explain why these factors are critical by demonstrating their respective impacts on WY through sensitivity analysis. This dual approach—combining both the changes in the factors and their elasticities—provides a more comprehensive understanding of the

drivers behind the observed changes in WY, ensuring that the results of the scenario analysis are both meaningful and robust.

# 3 Results

## 3.1 Changes in hydrometeorological variables

Fig. 2 demonstrates the trends of annual precipitation, air temperature, relative humidity, atmospheric pressure, solar radiation, and NDVI across China during 1982-2017. Annual precipitation change exhibited a clear spatial distribution pattern, specifically decreases in central China, including the middle reaches of the Yellow River and the Yangtze River basins, and increases in the northwest and southeast. Air temperature exhibited a consistent warming trend across China. In contrast, relative humidity generally decreased across most China. Atmospheric pressure remained relatively stable. Regarding solar radiation, decreases were in northern China, while an increase was in southern regions. The decreasing solar radiation in northern China is likely due to increased aerosol concentrations (Liang et al., 2024). NDVI showed a significant increasing trend, which indicates an overall enhancement in vegetation growth across China. This trend was especially prominent in central and eastern regions, including the Yellow River Basin and the Yangtze River Basin. In these regions, LULC changes, such as afforestation and agricultural practices, likely contributed to the observed increases in NDVI (Chen et al., 2019).

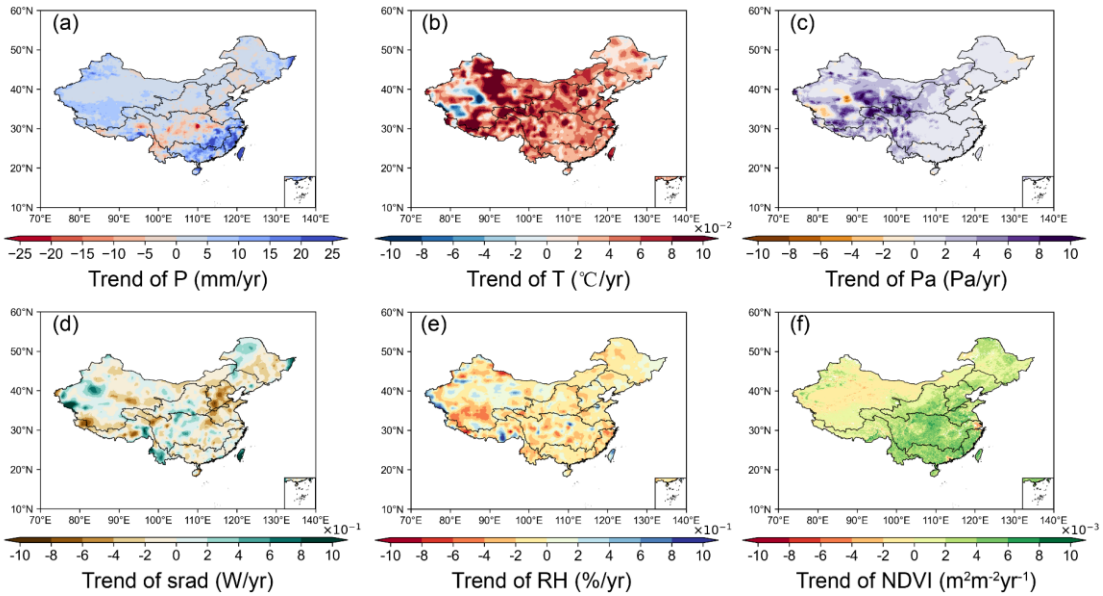


**Figure 2.** Spatial patterns of trends in annual climatic and vegetation variables during 1982–2017. (a) precipitation (mm/yr); (b) air temperature (°C/yr); (c) Atmospheric pressure (Pa/yr); (d) shortwave radiation (W/m$^2$/yr); (e) relative humidity (%/yr); (f) NDVI (yr$^{-1}$).

Significant changes in land use and land cover (LULC) occurred in China during 1982-2017, as illustrated in Fig. 3. Although the overall percentage distribution of major land cover types, namely grasslands, forests, croplands, and bare lands, remained relatively stable, these four categories dominated the landscape, with most changes concentrated within them. Notably, the transitions among these categories were characterized by mutual conversions, particularly from bare land to grasslands (Fig. 3). Spatially, the changes exhibited distinct regional patterns. In southern China, LULC changes were mainly characterized by the conversion of land to forests and grasslands. In contrast, the northeastern regions exhibited more complex transformations, with some areas shifting to bare land and croplands (Fig. 3).

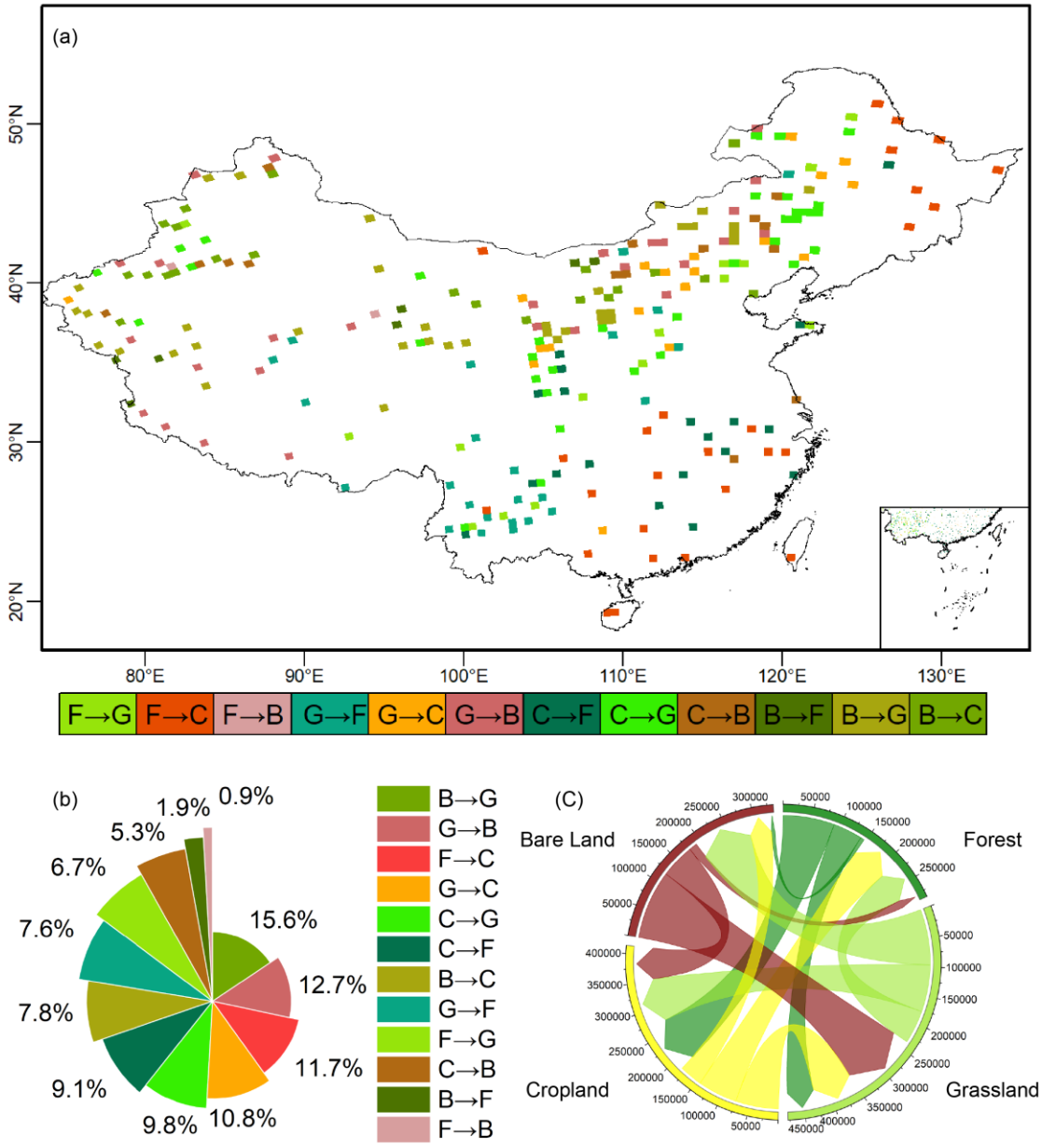


369

370 **Figure 3.** Land use and land cover (LULC) changes from 1982 to 2017. (a) Spatial
371 distribution of major conversion types among the four dominant LULC classes. F =
372 forest, G = grassland, C = cropland, and B = bare land. The arrow indicates the direction
373 of conversion from the original land-cover type to the converted type. (b) Percentage
374 share of each major conversion type in the total converted area (%). (c) Chord diagram
375 of the corresponding conversion flows, where the labels around the circle denote land-
376 cover classes, and the surrounding axis values indicate converted area (km²).

## 3.2 Performance of the improved CCW model

As shown in Fig. 4a and b, the observed annual water yield (WY) and the simulated annual WY by the improved CCW model showed strong linear correlations ($R^2$ = 0.7), with the regression line slope being 1.45, $R^2$ being 0.7, and RMSE being 9.54 mm/yr. By contrast, the initial model without WUE showed weaker skill (slope = 1.45 , $R^2$ = 0.68, RMSE = 9.62 mm/yr), indicating that explicitly representing [$CO_2$]-induced regulation of water-use efficiency measurably improves accuracy and reduces bias.

The estimated annual WY trends had distinct spatial patterns (Fig. 4c), which closely aligned with that of precipitation. Specifically, decrease trends in WY occurred in the central regions of the Yellow River Basin and the middle section of the Yangtze River Basin, while increase trends were found in other regions, with the southeast exhibiting the highest rate of increase.

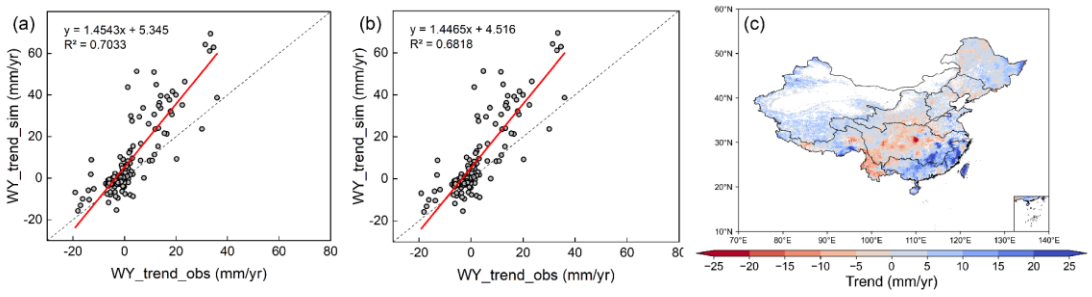


**Figure 4.** (a) Validation of simulated WY trend using the improved CCW model; (b) Validation of simulated WY trend using the initial CCW model; (c) Spatial distribution of WY trends under scenario S1(actual situation) during 1982–2017.

## 3.3 Attribution analysis of annual WY changes

Fig. 5 shows the distribution of WY changes caused by climate, vegetation, and [$CO_2$] changes, integrating both absolute magnitude (Fig. 5a,c,d) and relative dominance (Fig. 5b,d,f) of their contributions. Climate-driven WY changes exhibited marked spatial heterogeneity, with absolute increases exceeding 15 mm/yr in

southeastern China (Fig. 5a), corresponding to 60-90% relative contributions (Fig. 5b). Central basins showed contrasting declines of 0-6 mm/yr under climate forcing, while northeastern transitional zones displayed mixed positive/negative absolute changes (Fig. 5a) despite maintaining 40-70% relative climate dominance (Fig. 5b). This spatial heterogeneity aligned with precipitation change patterns (Fig. 2a).

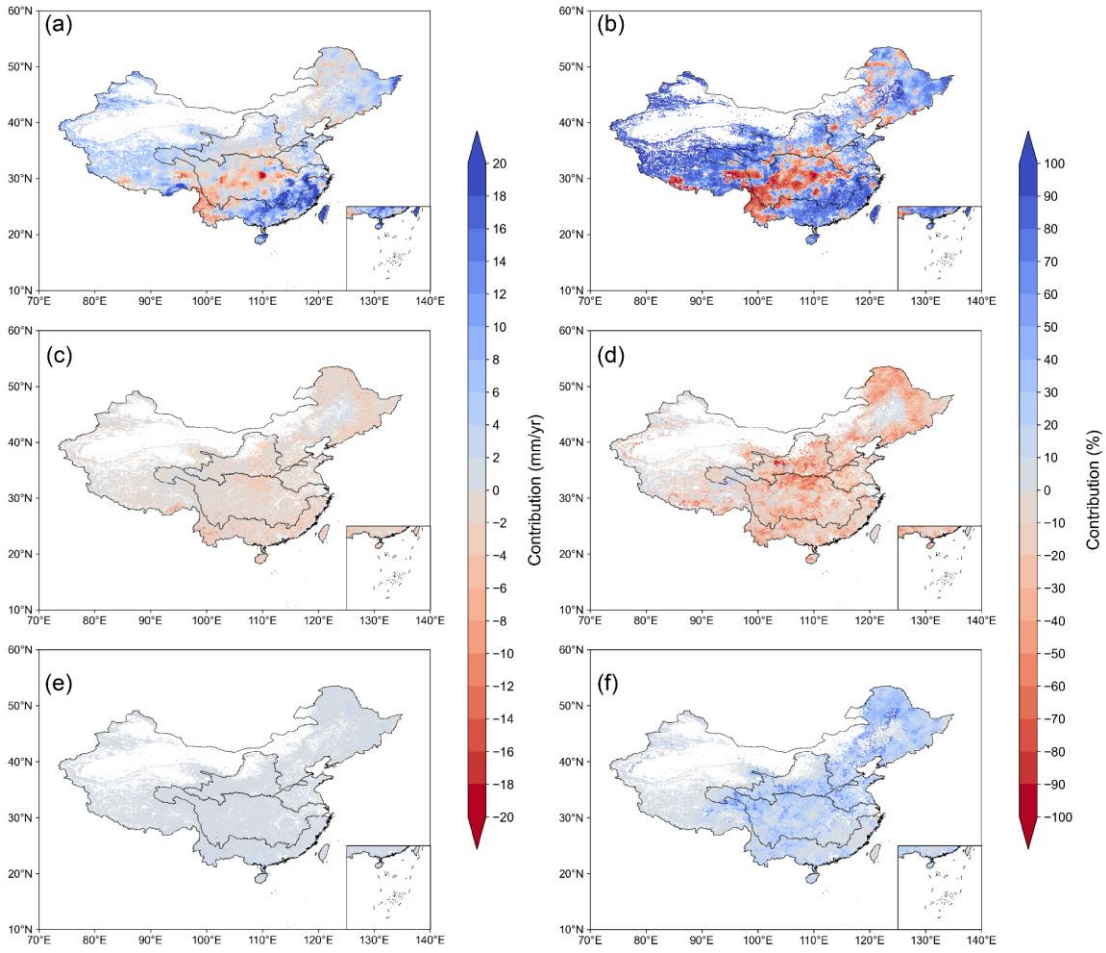


**Figure 5.** The absolute contributions of (a) climate, (c) vegetation, and (e) [$CO_2$], and the relative contributions of (b) climate, (d) vegetation, and (f) [$CO_2$] to changes in WY trends for 1982-2017.

Vegetation-mediated WY reductions reached 0-6 mm/yr (Fig. 5c), accompanied by 0-60% relative contributions (Fig. 5d). These effects originated from enhanced evapotranspiration through land-use changes and NDVI-based greening, particularly pronounced in central China. Specific regions in the Yangtze, Yellow, and northeastern rivers showed vegetation-driven relative contributions reaching 40-60% (Fig. 5d). [$CO_2$] effects generated limited direct absolute impacts (<5 mm/yr, Fig. 5e) but exerted 10-

40% relative influences (Fig. 5f) through stomatal closure mechanisms. This process partially counteracted vegetation-related WY losses in transitional climates like northeastern China, where competing drivers created complex ecohydrological interactions (Fig. 5).

Fig. 6 illustrated the spatial distribution of WY trend drivers over the past four decades. Climate change was the dominant factor of WY variation in more than 70% regions, mainly in the Northwest, Southwest, Southeast, Pearl River basins, and other parts of the Yangtze and Yellow River basins. Vegetation changes ranked as the secondary control, dominating WY changes in parts of the Yangtze, Yellow, Songhua, Liao, and Hai Rivers. Remarkably, it was shown that the region where vegetation and [$CO_2$] had the dominant influence mainly distributes within precipitation ranges of 400–1600 mm. $CO_2$-induced effects were least influential at a national scale. This three-tiered hierarchy—climate changes as the primary forcing, vegetation changes as the secondary control, and [$CO_2$] effects as a localized modifier—reveals how hydrological regimes govern the spatial succession of dominant drivers across China's diverse ecohydrological gradients.

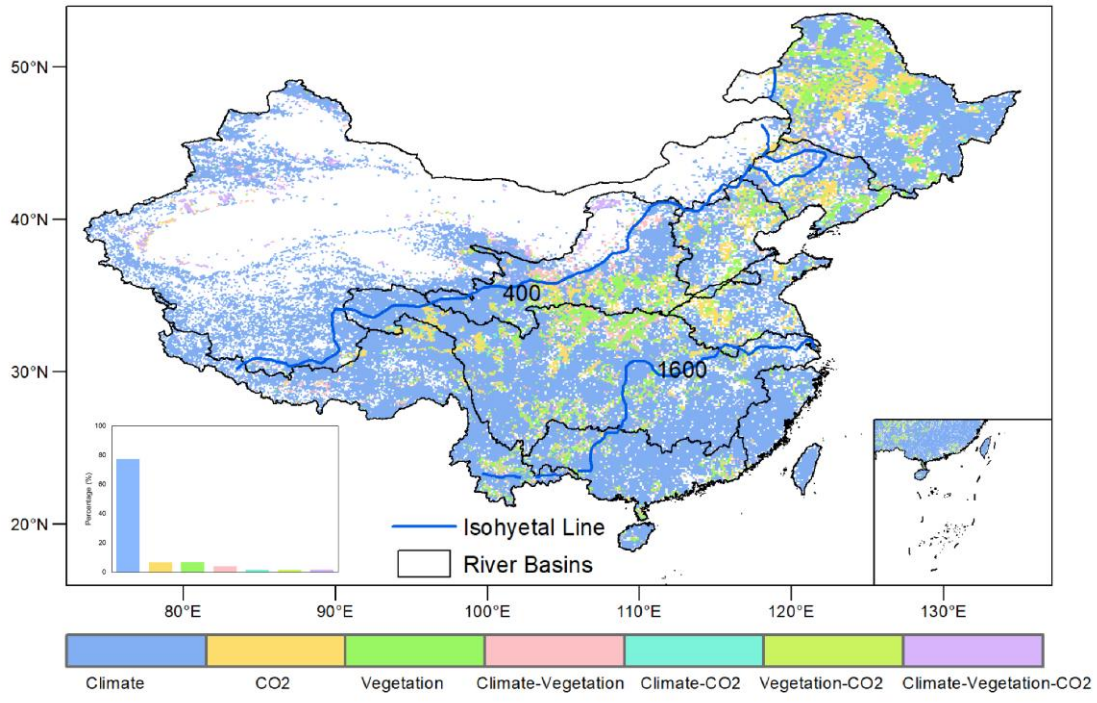

**Figure 6.** Spatial distributions of dominant factors controlling WY change. Driving factors include climate, vegetation, and [$CO_2$]. Climate: Areas where climate (e.g., precipitation, temperature) is the dominant factor influencing WY change; CO2: Areas where [$CO_2$] is the primary driver of WY change; Vegetation: Areas where vegetation changes (e.g., NDVI, LULC) primarily drive WY changes. Climate-Vegetation: Areas where both climate and vegetation jointly influence WY; Climate-CO2: Areas where both climate and [$CO_2$] jointly contribute to WY change; Vegetation-CO2: Areas where vegetation changes and [$CO_2$] jointly control WY; Climate-Vegetation-CO2: Areas where the combined effect of climate, vegetation, and [$CO_2$] jointly controls WY change. Additionally, the approximate isohyetal line shown in the figure were derived based on annual precipitation data from 1982 to 2017.

## 3.4 Elasticity of WY to main variables

The sensitivity of WY to precipitation (εP), NDVI (εNDVI), and [$CO_2$] ($\varepsilon CO_2$) exhibits distinct spatial patterns in (Fig. 7). Nationally averaged elasticity coefficients showed that a 10% increase in precipitation, [$CO_2$], and NDVI altered WY by 15.5% (εP=1.55), 5.5% ($\varepsilon CO_2$=0.55), and -4.4% (εNDVI=-0.44), respectively, indicating that, in terms of the sensitivity of runoff to changes in each factor, the ranking was precipitation > [$CO_2$] > NDVI.

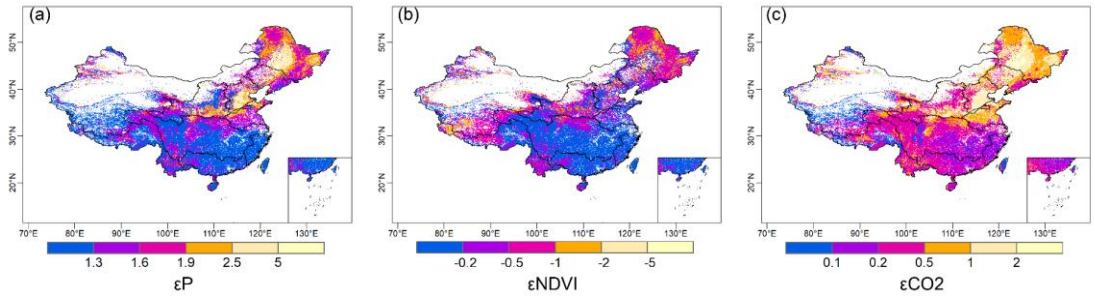


**Figure 7. S**patial distribution of elasticity coefficients of WY relative to changes in hydrological variables such as (a) annual precipitation, (b) NDVI, and (c) [$CO_2$].

The elasticity coefficients of precipitation (εP), [$CO_2$] ($\varepsilon CO_2$), and vegetation (|εNDVI|) all exhibited a coherent latitudinal decline across China's river basins, showing systematically higher sensitivity in northern regions than southern counterparts. Quantitatively, εP decreased from 2.09 in the Songhua River basin to 1.15 in the Southeastern Basin, accompanied by similar reductions in |εNDVI| (from 0.76 to 0.13) and $\varepsilon CO_2$ (from 1.08 to 0.16) (Table 3).

A distinct abrupt transition zone in elasticity coefficients was identified around 33°N, closely aligning with China's traditional North-South physiographic divide. Around the zone, elasticity coefficients exhibited an abrupt decline from the Yellow River Basin to the Yangtze River Basin. Specifically, the Yellow River Basin showed higher sensitivities to precipitation (εP=1.87), [$CO_2$] ($\varepsilon CO_2$=0.86), and NDVI (εNDVI=-0.53), which were approximately 1.4, 2.8, and 2.8 times greater, respectively, than those in the Yangtze River Basin (εP=1.31, $\varepsilon CO_2$=0.31, εNDVI=-0.19).

**Table 3**. Elasticity Coefficients of Runoff to Precipitation, NDVI, and $CO_2$ in Different Watersheds

| Dataset | εP | εNDVI | $\varepsilon CO_2$ |
|---|---|---|---|
| **Songhua River basin** | 2.09 | -0.76 | 1.08 |
| **Hai River basin** | 2.13 | -0.44 | 1.12 |
| **Yellow River basin** | 1.87 | -0.53 | 0.86 |
| **Yangtze River Basin** | 1.31 | -0.19 | 0.31 |
| **Huai River basin** | 1.64 | -0.18 | 0.63 |
| **Pearl River basin** | 1.25 | -0.17 | 0.25 |
| **Southeast Rivers** | 1.15 | -0.13 | 0.15 |

Note: Some LULC types were excluded from the analysis. Due to many missing data points, the Liao River, Southwest, and Northwest river basins were also omitted.

# 4 Discussion

## 4.1 Strength of the attribution analysis framework

To address limitations in current methods for analysing the effects of climate, vegetation, and [$CO_2$] on runoff changes, we developed an attribution analysis framework based on the improved CCW model. This framework has been improved in three aspects. Firstly, the explicit and mechanistic integration of vegetation dynamics and [$CO_2$] effects overcomes the oversimplifications inherent in conventional approaches. Traditional Budyko-based frameworks often attribute vegetation effects to temporal variations in the Budyko parameter (n) by either statistically regressing the Budyko parameter against vegetation proxies such as NDVI (Liu et al., 2024; Tan et al., 2023) or simplistically equating the Budyko parameter to vegetation effects (Li et

al., 2020b; Zhou et al., 2023). Such approaches conflate structural vegetation changes (e.g., leaf area index) with physiological adjustments (e.g., $CO_2$-induced stomatal closure), thereby obscuring the independent roles of vegetation dynamics and [$CO_2$]. For example, while rising [$CO_2$] levels directly reduce stomatal conductance and transpiration, Budyko-based studies often misinterpret this effect as part of the the Budyko parameter's variability, erroneously attributing it to vegetation changes (Zeng et al., 2020). In contrast, our framework mechanistically separates these pathways by explicitly describing the stomatal conductance–WUE relationship based on plant physiological theory. Elevated [$CO_2$] reduces stomatal aperture, thereby lowering stomatal conductance and transpiration flux while only modestly increasing carbon assimilation, leading to an overall enhancement in water-use efficiency (WUE). This process is represented by the Medlyn-type stomatal conductance model (Medlyn et al., 2011), which links photosynthetic rate (A), transpiration (T), and vapor pressure deficit (D) as:

$$\frac{A}{T} = \frac{C_a P_a}{1.6\left(D + g_1\sqrt{D}\right)}$$

where $C_a$ is atmospheric $CO_2$ concentration, $P_a$ is air pressure, D is vapor pressure deficit, and $g_1$ is an empirical slope parameter that quantifies plant sensitivity to $CO_2$ and humidity. According to this formulation, rising [$CO_2$] increases while reducing stomatal conductance, which in turn suppresses transpiration more strongly than photosynthesis, resulting in higher WUE. This mechanistic representation enables our framework to capture the direct physiological $CO_2$ effect on evapotranspiration, which is otherwise masked in Budyko-type models where $CO_2$ impacts are embedded implicitly in PET or the "n" parameter.

Secondly, unlike Budyko-based methods that indirectly represent [$CO_2$] impacts through adjustments to potential evapotranspiration (PET)—a practice conflating [$CO_2$] effects with meteorological drivers like radiation and wind—our framework explicitly quantifies $CO_2$'s physiological influence on actual evapotranspiration (AET) by

mechanistically modeling its role in stomatal conductance and water-use efficiency (WUE). Elevated [$CO_2$] reduces stomatal conductance and transpiration while moderately enhancing carbon assimilation, partially offsetting water losses associated with vegetation greening. For example, our results show that reduction in transpiration due to $CO_2$-driven stomatal closure offsets water losses, a mechanism entirely masked in Budyko frameworks where [$CO_2$] effects are ambiguously embedded in PET adjustments or erroneously attributed to vegetation structural changes via the "n" parameter (Liu et al., 2024). This coupled regulation clarified how water and energy jointly constrain evapotranspiration, particularly in 400-1600 mm precipitation zones. In these regions, vegetation growth enhanced transpiration and root water uptake until increasing atmospheric aridity imposed physiological constraints, while rising [$CO_2$] partially counteracted this effect by improving water-use efficiency through stomatal closure. As a result, the framework provided a more mechanistically grounded understanding of how [$CO_2$] modulates ecosystem water use and hydrological responses at regional scales.

Compared with the original CCW model using static UWUE, the improved framework does not merely provide a modest statistical improvement. Its main advance is that it allows WUE to vary dynamically with [$CO_2$], VPD, and canopy structure, thereby explicitly representing the physiological regulation of ET by rising [$CO_2$]. This makes it possible to distinguish LAI (vegetation structural) water consumption from [$CO_2$]-induced stomatal water-saving effects, which is essential for interpreting why WY responses differ across regions and why [$CO_2$] can partly offset vegetation-related WY reductions.

Thirdly, while numerous studies have conducted runoff attribution analysis at the basin scale (Liu et al., 2024, 2017; Yang et al., 2022), our grid-scale approach transcends the spatial constraints of fixed watershed boundaries by resolving regional heterogeneity in hydrological drivers. Conventional basin-aggregated methods obscure critical intra-basin differences—for instance, our analysis reveals that grids in the upper

Yangtze River basin, where precipitation change dominates runoff trends, necessitate climate scenario-based water resource planning. In contrast, mid-basin grids with significant NDVI-driven greening exhibit pronounced WY reductions, highlighting the need for vegetation management strategies that restrict excessive afforestation in water-sensitive areas (Sun et al., 2022; Yang et al., 2021). By decoupling analysis from rigid watershed boundaries, our framework enables targeted strategies such as restricting reforestation in water-stressed grids or selecting $CO_2$-adapted vegetation species, thereby aligning management actions with localized climate-vegetation-hydrology interactions.

## 4.2 New insights into attribution analysis

Our findings highlighted climate change as the dominant driver of water yield (WY) changes (contributing >70%), consistent with other assessments (Table 4), yet reveal critical regional divergences. Climate impacts dominated in the Northwest and Southwest River Basins, as well as parts of the Yangtze, Yellow, Southeast, and Pearl River Basins, while vegetation and [$CO_2$] effects prevailed in central China (parts of the Yangtze, Yellow, Songhua, Liao, and Hai River basin)—a spatial pattern slightly distinct from earlier studies. Although previous studies identified human activities as the primary driver in some northern basins (Liao, Hai, and Yellow River Basins) ((Yang et al., 2022), their long-term study (1965-2018) diluted the gradually strengthening vegetation signals after 2000 mentioned in other studies (Liu et al., 2017; Sun et al., 2023) through time-averaging. Our findings now confirm the emerging importance of vegetation dynamics in southern basins like the Yangtze through our symmetric 1982-2017 study period. This basin-scale contrast is also consistent with a broader hydroclimatic gradient, as vegetation and [$CO_2$] effects become relatively more important in the intermediate 400–1600 mm precipitation zone. Although the improvement in overall model performance is modest, the main value of introducing dynamic WUE is not limited to statistical enhancement. More importantly, this

refinement allows the improved CCW model to explicitly represent the physiological effect of rising [$CO_2$] on evapotranspiration, which cannot be resolved by the original static-UWUE formulation. As a result, the model can distinguish vegetation-driven increases in water consumption from [$CO_2$]-induced stomatal water-saving effects, thereby providing new insight into why WY responses differ across regions and why [$CO_2$] can partially offset vegetation-related WY reductions, especially in transitional hydroclimatic zones.

**Table 4.** Comparative studies of the contribution of climate variability and vegetation to runoff changes.

| Reference | Study region | Study period | Method/Model | Driving factors |
|---|---|---|---|---|
| **(Wei et al., 2024)** | Global | 1981-2020 | Trendy phase 11 +ROF | Climate change |
| **(Liu et al., 2024)** | Global | 1984-2010; 2000-2100 | Improved Budyko | Precipitation |
| **(Zhou et al., 2023)** | Global | 1850-2014; 2015-2100 | Improved Budyko + CMIP6 | Land surface changes |
| **(Tan et al., 2023)** | Global | 2003-2016; 1982-2016 | Improved Budyko | Effective precipitation |
| **(Yang et al., 2022)** | China | 1965-2018 | Budyko | P: Northwest river basin, Southwest river basin, Yangtze river basin, Southeast river basin, and Pearl river basin;<br>Budyko parameter (n): Liaohe river basin, Haihe river basin, Yellow river Basin, Songhuajiang river basin, and Huaihe river basin |
| **(Zhang et al., 2022b)** | Yangtze River | 2001-2018 | CCW Model | Climate variability |
| **(Chen et al., 2022)** | Six river basins in China | 1982-2015 | Gray Relational Analysis (GRA) | Precipitation |
| **(Zhai and Tao, 2021)** | China | 1982-2015 | VIC Model | Climate change |
| **(Li et al., 2020a)** | Yihe River | 1960-2013 | SWAT+WRF | Climate variability |
| **(Shen et al., 2017)** | China | 1960-2010 | Budyko | Underlying surface change (n): the Songhua Basin, the Liaohe Basin and the Haihe Basin;<br>Climate change: in other basins. |

Elasticity analysis (Section 3.4) revealed distinct sensitivities of WY to environmental drivers: precipitation exhibited the highest elasticity coefficient for the whole China ($\varepsilon P = 1.55$), followed by $CO_2$ ($\varepsilon CO_2 = 0.55$) and NDVI ($\varepsilon NDVI = -0.44$).

However, spatial analysis showed that vegetation and [$CO_2$] collectively dominated WY changes in 400–1600 mm precipitation zones, despite their lower sensitivity rankings. The joint effect of elasticity and the magnitude of driver change determines each driver's net contribution. In the 400–1600 mm precipitation zones, NDVI displayed (Fig. 8) a larger relative temporal variation compared with precipitation, which fluctuated within a narrower range. Consequently, vegetation's stronger relative change amplified its hydrological influence, overriding its lower elasticity. Similarly, $CO_2$'s historical impact was constrained by its slow accumulation rate (0.49%/yr), yet its relatively high elasticity positions it as a latent driver.

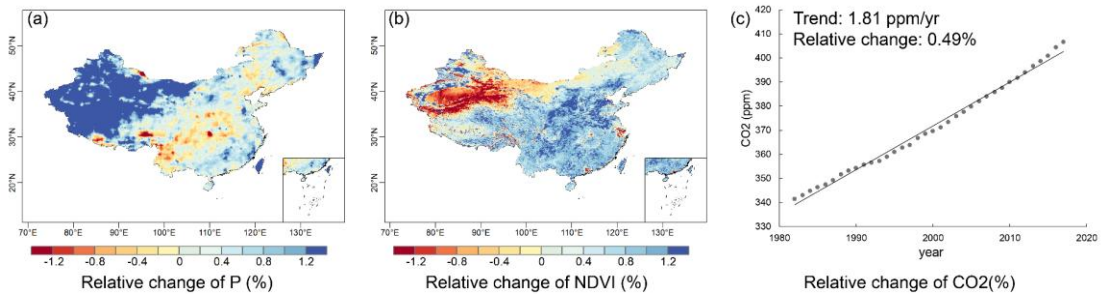


**Figure 8.** Spatial distribution of relative changes of different variables: (a) annual precipitation, and (b) NDVI.

This historical constraint, however, belied $CO_2$'s transformative potential under intensified forcing scenarios. CMIP6 SSP585 projections indicate [$CO_2$] will rise at 2.34%/yr—nearly fivefold faster than historical rates (Cheng et al., 2022). Using the historical elasticity coefficient as a simple sensitivity-based approximation, $CO_2$'s elasticity would drive a +1.29% annual WY increase, eclipsing both vegetation greening effects and even surpassing precipitation-driven changes in some regions. However, this estimate assumes that the historical [$CO_2$] elasticity remains unchanged and does not account for possible counteracting effects such as rising VPD, drought stress, or saturation of WUE under elevated [$CO_2$] (Adams et al., 2020; Li et al., 2023). Nevertheless, the result suggests that [$CO_2$] may become a more important hydrological

modifier under strong future forcing, particularly in the 400–1600 mm precipitation zones.

From a policy perspective, these spatial contrasts have distinct implications for regional water management. In vegetation-dominated regions such as the Yangtze and Huang river basins, enhancing ecosystem-based restoration, optimizing vegetation composition, and preventing overgreening that may suppress runoff should be prioritized. Conversely, in climate-dominated areas such as Northwest and Southeast China, adaptive measures emphasizing precipitation variability, water storage capacity, and drought resilience are crucial. Recognizing and tailoring water management strategies to these driver-specific regimes can enhance the effectiveness of both ecological restoration and climate adaptation programs across China.

## 4.3 Uncertainty in attribution analysis

This study provides valuable insights into the relationship between water resources management and environmental changes, which can guide environmental management strategies. However, several limitations exist that need to be addressed in future work to improve the accuracy and robustness of the results.

Firstly, the adopted WUE formulation is defined at the ecosystem scale, but the present implementation simplifies the interception term by assuming $f_i = 0$. Soil evaporation is still implicitly represented through the LAI-based partitioning term, whereas canopy interception is not explicitly allowed to vary across space or time. This simplification may bias the absolute magnitude of ET and WY, particularly in humid and forested regions, although its influence on long-term WY trends is expected to be smaller than on short-term hydrological fluxes. Despite this, considering the small change of $f_i$ in the current year (Zhao et al., 2022), its influence on runoff trends is negligible in our study (Cheng et al., 2017). However, future work should prioritize its calculation to improve the precision of WY estimates.

Secondly, the complex interrelationships among climate, vegetation, and [$CO_2$] cannot be fully disentangled. Vegetation exhibits tight biophysical interactions and feedback with climate, making it difficult to separate the impacts of climate change, vegetation dynamics, and [$CO_2$] on hydrological responses in a strictly independent manner. Changes in vegetation, such as NDVI, reflect a combination of climate change, human activities (e.g., reforestation and irrigation), and natural vegetation growth. Additionally, vegetation greening in upwind regions can increase atmospheric moisture, potentially enhancing precipitation downwind (Zhang et al., 2021a), which may counteract some of the negative impacts of increased evapotranspiration on local WY. Although the climate data used in our model may implicitly capture some of these feedbacks, they cannot be explicitly separated in this analysis. Consequently, our results represent an attempt to estimate the direct first-order net impacts of climate, vegetation greening, and [$CO_2$] increase on WY (Zhang et al., 2021b). Future research should adopt more comprehensive models that consider soil-vegetation-atmosphere interactions to better differentiate the contributions of each driving factor to WY.

Thirdly, the improved CCW model does not incorporate certain human activities, such as large-scale irrigation, groundwater pumping, and reservoir regulation, which also limits the assumption of WY = P − ET with negligible storage change. This assumption is mainly appropriate at the annual scale and becomes less reliable in regions where long-term groundwater depletion or reservoir operation substantially alters water storage and runoff routing. For instance, irrigation can sustain vegetation greening during dry seasons, potentially amplifying the vegetation–climate feedback on water yield. Incorporating such anthropogenic processes into the CCW framework through coupled irrigation and water management modules would enable more comprehensive attribution analyses in future studies. Our research also excludes water bodies and built-up land. While urbanization can increase flood risks due to the growing proportion of impervious surfaces (Wasko and Sharma, 2017), these land-use changes represent a small portion of China’s land area.

Finally, the future impact of vegetation greening on hydrological dynamics will depend on projected climate warming and drying trends, the persistence of vegetation greening, [$CO_2$] changes, and the complex feedbacks between climate, soil, and vegetation. In particular, the simple elasticity-based SSP585 estimate of the [$CO_2$] effect does not account for concurrent changes in VPD or possible saturation of WUE under elevated [$CO_2$] and drought stress, which adds uncertainty to the future WY response. These interactions require long-term study, and future research will involve more extensive monitoring to better capture these evolving dynamics.

# 5 Conclusions

In this study, we improved the CCW model incorporating dynamic water use efficiency (WUE) calculation to explicitly represent $CO_2$-physiological feedback on water yield. This mechanistic improvement enabled comprehensive national-scale assessment quantifying the relative contributions of climate forcing, vegetation structural changes, and $CO_2$-driven stomatal regulation to water yield (WY) dynamics in China. The main conclusions are as follows:

The improved CCW model effectively simulated WY variations in most basins under increased [$CO_2$] scenarios, demonstrating its applicability and reliability in modeling WY changes.

Climate change, particularly variations in precipitation, emerged as the primary driver influencing WY, displaying significant regional disparities in its effects. Vegetation changes constituted the second most critical factor, predominantly resulting in WY reduction, notably in central China. While the effect of $CO_2$-induced stomatal closure on WY was comparatively minor. Spatial analysis aligned with isohyetal lines further revealed that vegetation change and [$CO_2$] exerted greater influence within the 400–1600 mm precipitation range.

The elasticity analysis of WY indicated that northern basins exhibit higher sensitivity to influencing factors, whereas southern basins demonstrate relatively lower

elasticity. Specifically, the absolute elasticity coefficients for the whole China were ranked in descending order as follows: precipitation > [$CO_2$] > NDVI. Thus, accelerating [$CO_2$] rise (2.34% /yr under SSP585) will amplify its hydrological role, potentially elevating $CO_2$-driven WY increases to +1.29% annually by 2100, surpassing climate and vegetation impacts, although this estimate does not account for concurrent VPD changes or possible WUE saturation.

These insights provide a nuanced understanding of regional hydrological responses, essential for sustainable water resource management under changing environmental conditions.

## Acknowledgements

This research was supported by the China National Key R&D Program (grant no. 2024YFF1306901) and Open Research Fund Program of the State Key Laboratory of Hydroscience and Engineering (grant no. sklhse-KF-2026-A-03).

## Data Availability Statement

Datasets used for driving models were obtained from different sources described in Table 1. All the data related to our results in this study can be found online: the NDVI data (https://doi.org/10.6084/m9.figshare.c.7002225.v1); the climate data (https://www.tpdc.ac.cn/zh-hans/data/8028b944-daaa-4511-8769-965612652c49/); the land use and land cover (LULC) data (https://zenodo.org/records/8239305) (Liu et al., 2023); and the [$CO_2$] (http://cdiac.esd.ornl.gov/ftp/trends/co2/maunaloa.co2), except for the streamflow records for hydrological gauging stations, which are available upon reasonable request.

## Author contributions

HS designed the study, developed the model code, did the simulation experiments, and wrote the first draft of the paper. HY designed the research and edited the manuscript. CL provided feedback on the results and edited the manuscript.

## Competing interests

The contact author has declared that neither they nor their co-authors have any competing interests.

# Reference


Adams, M. A., Buckley, T. N., and Turnbull, T. L.: Diminishing CO2-driven gains in water-use efficiency of global forests, Nat. Clim. Chang., 10, 466–471, https://doi.org/10.1038/s41558-020-0747-7, 2020.

Chen, C., Park, T., Wang, X., Piao, S., Xu, B., Chaturvedi, R. K., Fuchs, R., Brovkin, V., Ciais, P., Fensholt, R., Tømmervik, H., Bala, G., Zhu, Z., Nemani, R. R., and Myneni, R. B.: China and India lead in greening of the world through land-use management, Nat Sustain, 2, 122–129, https://doi.org/10.1038/s41893-019-0220-7, 2019.

Chen, S., Fu, Y. H., Geng, X., Hao, Z., Tang, J., Zhang, X., Xu, Z., and Hao, F.: Influences of Shifted Vegetation Phenology on Runoff Across a Hydroclimatic Gradient, Front. Plant Sci., 12, 802664, https://doi.org/10.3389/fpls.2021.802664, 2022.

Cheng, L., Zhang, L., Wang, Y.-P., Canadell, J. G., Chiew, F. H. S., Beringer, J., Li, L., Miralles, D. G., Piao, S., and Zhang, Y.: Recent increases in terrestrial carbon uptake at little cost to the water cycle, Nat Commun, 8, 110, https://doi.org/10.1038/s41467-017-00114-5, 2017.

Cheng, W., Dan, L., Deng, X., Feng, J., Wang, Y., Peng, J., Tian, J., Qi, W., Liu, Z., Zheng, X., Zhou, D., Jiang, S., Zhao, H., and Wang, X.: Global monthly gridded atmospheric carbon dioxide concentrations under the historical and future scenarios, Sci Data, 9, 83, https://doi.org/10.1038/s41597-022-01196-7, 2022.

Fu, J., Liu, B., Wang, W., and Fei, E. X.: Evaluating main drivers of runoff changes across China from 1956 to 2000 by using different budyko-based elasticity methods, Journal of Environmental Management, 329, 117070, https://doi.org/10.1016/j.jenvman.2022.117070, 2023.

Gan, G., Liu, Y., and Sun, G.: Understanding interactions among climate, water, and vegetation with the Budyko framework, Earth-Science Reviews, 212, 103451, https://doi.org/10.1016/j.earscirev.2020.103451, 2021.

Gutman, G. and Ignatov, A.: The derivation of the green vegetation fraction from NOAA/AVHRR data for use in numerical weather prediction models, International Journal of Remote Sensing, 19, 1533–1543, https://doi.org/10.1080/014311698215333, 1998.

He, J., Yang, K., Tang, W., Lu, H., Qin, J., Chen, Y., and Li, X.: The first high-resolution meteorological forcing dataset for land process studies over China, Sci Data, 7, 25, https://doi.org/10.1038/s41597-020-0369-y, 2020.

Howell, T. A. and Dusek, D. A.: Comparison of Vapor-Pressure-Deficit Calculation Methods—Southern High Plains, J. Irrig. Drain Eng., 121, 191–198, https://doi.org/10.1061/(ASCE)0733-9437(1995)121:2(191), 1995.

Jia, Y., Li, C., Yang, H., Yang, W., and Liu, Z.: Assessments of three evapotranspiration products over China using extended triple collocation and water balance methods, Journal of Hydrology, 614, 128594, https://doi.org/10.1016/j.jhydrol.2022.128594, 2022.

Jiao, Y., Lei, H., Yang, D., Huang, M., Liu, D., and Yuan, X.: Impact of vegetation dynamics on hydrological processes in a semi-arid basin by using a land surface-hydrology coupled model, Journal of Hydrology, 551, 116–131, https://doi.org/10.1016/j.jhydrol.2017.05.060, 2017.

Lammertsma, E. I., Boer, H. J. D., Dekker, S. C., Dilcher, D. L., Lotter, A. F., and Wagner-Cremer, F.: Global $CO_2$ rise leads to reduced maximum stomatal conductance in Florida vegetation, Proc. Natl. Acad. Sci. U.S.A., 108, 4035–4040, https://doi.org/10.1073/pnas.1100371108, 2011.

Li, B., Shi, X., Lian, L., Chen, Y., Chen, Z., and Sun, X.: Quantifying the effects of climate variability, direct and indirect land use change, and human activities on runoff, Journal of Hydrology, 584, 124684, https://doi.org/10.1016/j.jhydrol.2020.124684, 2020a.

Li, F., Xiao, J., Chen, J., Ballantyne, A., Jin, K., Li, B., Abraha, M., and John, R.: Global water use efficiency saturation due to increased vapor pressure deficit, Science, 381, 672–677, https://doi.org/10.1126/science.adf5041, 2023.

Li, H., Shi, C., Zhang, Y., Ning, T., Sun, P., Liu, X., Ma, X., Liu, W., and Collins, A. L.: Using the Budyko hypothesis for detecting and attributing changes in runoff to climate and vegetation change in the soft sandstone area of the middle Yellow River basin, China, Science of The Total Environment, 703, 135588, https://doi.org/10.1016/j.scitotenv.2019.135588, 2020b.

Li, H., Cao, Y., Xiao, J., Yuan, Z., Hao, Z., Bai, X., Wu, Y., and Liu, Y.: A daily gap-free normalized difference vegetation index dataset from 1981 to 2023 in China, Sci Data, 11, 527, https://doi.org/10.1038/s41597-024-03364-3, 2024a.

Li, X., Xu, X., Sonnenborg, T. O., Andreasen, M., and He, C.: Effect of ecological restoration on evapotranspiration and water yield in the agro-pastoral ecotone in northern China during 2000–2018, Journal of Hydrology, 638, 131531, https://doi.org/10.1016/j.jhydrol.2024.131531, 2024b.

Liang, L., Han, Z., Chen, W., Li, J., Liang, M., and Shen, S.: The source, transport, deposition and direct radiative effect of mineral dust over western China: A modeling

778 study of July 2022 with focus on the Tibetan Plateau, Atmospheric Research, 311,
779 107708, https://doi.org/10.1016/j.atmosres.2024.107708, 2024.

780 Liu, C., Feng, S., Zhang, Q., Hu, J., Ma, N., Ci, H., Kong, D., and Gu, X.: Critical
781 influence of vegetation response to rising CO2 on runoff changes, Science of The Total
782 Environment, 906, 167717, https://doi.org/10.1016/j.scitotenv.2023.167717, 2024.

783 Liu, J., Zhang, Q., Singh, V. P., and Shi, P.: Contribution of multiple climatic variables
784 and human activities to streamflow changes across China, Journal of Hydrology, 545,
785 145–162, https://doi.org/10.1016/j.jhydrol.2016.12.016, 2017.

786 Ma, T., Wang, T., Yang, D., and Yang, S.: Impacts of vegetation restoration on water
787 resources and carbon sequestration in the mountainous area of Haihe River basin, China,
788 Science of The Total Environment, 869, 161724,
789 https://doi.org/10.1016/j.scitotenv.2023.161724, 2023.

790 Medlyn, B. E., Duursma, R. A., Eamus, D., Ellsworth, D. S., Prentice, I. C., Barton, C.
791 V. M., Crous, K. Y., De Angelis, P., Freeman, M., and Wingate, L.: Reconciling the
792 optimal and empirical approaches to modelling stomatal conductance: RECONCILING
793 OPTIMAL AND EMPIRICAL STOMATAL MODELS, Global Change Biology, 17,
794 2134–2144, https://doi.org/10.1111/j.1365-2486.2010.02375.x, 2011.

795 Montibeller, B., Marshall, M., Mander, Ü., and Uuemaa, E.: Increased carbon
796 assimilation and efficient water usage may not compensate for carbon loss in European
797 forests, Commun Earth Environ, 3, 194, https://doi.org/10.1038/s43247-022-00535-1,
798 2022.

799 Mu, S., Zhou, S., Chen, Y., Li, J., Ju, W., and Odeh, I. O. A.: Assessing the impact of
800 restoration-induced land conversion and management alternatives on net primary
801 productivity in Inner Mongolian grassland, China, Global and Planetary Change, 108,
802 29–41, https://doi.org/10.1016/j.gloplacha.2013.06.007, 2013.

803 Nkiaka, E., Bryant, R. G., and Dembélé, M.: Quantifying Sahel Runoff Sensitivity to
804 Climate Variability, Soil Moisture and Vegetation Changes Using Analytical Methods,
805 Earth Syst Environ, 9, 491–504, https://doi.org/10.1007/s41748-024-00464-3, 2025.

806 Ogutu, B. O., D'Adamo, F., and Dash, J.: Impact of vegetation greening on carbon and
807 water cycle in the African Sahel-Sudano-Guinean region, Global and Planetary Change,
808 202, 103524, https://doi.org/10.1016/j.gloplacha.2021.103524, 2021.

809 Peng, H., Tague, C., and Jia, Y.: Evaluating the eco-hydrologic impacts of reforestation
810 in the Loess Plateau, China, using an eco-hydrologic model, Ecohydrology, 9, 498–513,
811 https://doi.org/10.1002/eco.1652, 2016.

Piao, S., Friedlingstein, P., Ciais, P., De Noblet-Ducoudré, N., Labat, D., and Zaehle, S.: Changes in climate and land use have a larger direct impact than rising $CO_2$ on global river runoff trends, Proc. Natl. Acad. Sci. U.S.A., 104, 15242–15247, https://doi.org/10.1073/pnas.0707213104, 2007.

Rahman, G., Farooq, U., Jung, M.-K., and Kwon, H.-H.: Spatiotemporal vegetation dynamics in South Asia (2001-2023): roles of climate and anthropogenic activities, Geosci. Lett., 12, 31, https://doi.org/10.1186/s40562-025-00403-8, 2025.

Running, S. W., Thornton, P. E., Nemani, R., and Glassy, J. M.: Global Terrestrial Gross and Net Primary Productivity from the Earth Observing System, in: Methods in Ecosystem Science, edited by: Sala, O. E., Jackson, R. B., Mooney, H. A., and Howarth, R. W., Springer New York, New York, NY, 44–57, https://doi.org/10.1007/978-1-4612-1224-9_4, 2000.

Serrano-Notivoli, R., Martínez-Salvador, A., García-Lorenzo, R., Espín-Sánchez, D., and Conesa-García, C.: Rainfall–runoff relationships at event scale in western Mediterranean ephemeral streams, Hydrol. Earth Syst. Sci., 26, 1243–1260, https://doi.org/10.5194/hess-26-1243-2022, 2022.

Shen, Q., Cong, Z., and Lei, H.: Evaluating the impact of climate and underlying surface change on runoff within the Budyko framework: A study across 224 catchments in China, Journal of Hydrology, 554, 251–262, https://doi.org/10.1016/j.jhydrol.2017.09.023, 2017.

Sims, D. A., Rahman, A. F., Cordova, V. D., Baldocchi, D. D., Flanagan, L. B., Goldstein, A. H., Hollinger, D. Y., Misson, L., Monson, R. K., Schmid, H. P., Wofsy, S. C., and Xu, L.: Midday values of gross CO2 flux and light use efficiency during satellite overpasses can be used to directly estimate eight-day mean flux, Agricultural and Forest Meteorology, 131, 1–12, https://doi.org/10.1016/j.agrformet.2005.04.006, 2005.

Sun, W., Ding, X., Su, J., Mu, X., Zhang, Y., Gao, P., and Zhao, G.: Land use and cover changes on the Loess Plateau: A comparison of six global or national land use and cover datasets, Land Use Policy, 119, 106165, https://doi.org/10.1016/j.landusepol.2022.106165, 2022.

Sun, X., Dong, Q., and Zhang, X.: Attribution analysis of runoff change based on Budyko-type model with time-varying parameters for the Lhasa River Basin, Qinghai–Tibet Plateau, Journal of Hydrology: Regional Studies, 48, 101469, https://doi.org/10.1016/j.ejrh.2023.101469, 2023.

Tan, X., Tan, X., Liu, B., and Huang, Z.: Contribution of changes in vegetation composition and climate variability on streamflow across the global watersheds, CATENA, 232, 107394, https://doi.org/10.1016/j.catena.2023.107394, 2023.

Tan, X., Jia, Y., Yang, D., Niu, C., and Hao, C.: Impact ways and their contributions to vegetation-induced runoff changes in the Loess Plateau, Journal of Hydrology: Regional Studies, 51, 101630, https://doi.org/10.1016/j.ejrh.2023.101630, 2024.

Wang, D. L., Feng, H. M., Zhang, B. Z., Wei, Z., and Tian, Y. L.: Quantifying the impacts of climate change and vegetation change on decreased runoff in china's yellow river basin, Ecohydrology & Hydrobiology, 22, 310–322, https://doi.org/10.1016/j.ecohyd.2021.10.002, 2022.

Wasko, C. and Sharma, A.: Global assessment of flood and storm extremes with increased temperatures, Sci Rep, 7, 7945, https://doi.org/10.1038/s41598-017-08481-1, 2017.

Wei, H., Zhang, Y., Huang, Q., Chiew, F. H. S., Luan, J., Xia, J., and Liu, C.: Direct vegetation response to recent CO2 rise shows limited effect on global streamflow, Nat Commun, 15, 9423, https://doi.org/10.1038/s41467-024-53879-x, 2024.

Xiao, M., Gao, M., Vogel, R. M., and Lettenmaier, D. P.: Runoff and Evapotranspiration Elasticities in the Western United States: Are They Consistent With Dooge's Complementary Relationship?, Water Resources Research, 56, e2019WR026719, https://doi.org/10.1029/2019WR026719, 2020.

Xu, X., Yang, D., Yang, H., and Lei, H.: Attribution analysis based on the Budyko hypothesis for detecting the dominant cause of runoff decline in Haihe basin, Journal of Hydrology, 510, 530–540, https://doi.org/10.1016/j.jhydrol.2013.12.052, 2014.

Xu, Z., Jiang, Y., Jia, B., and Zhou, G.: Elevated-CO2 Response of Stomata and Its Dependence on Environmental Factors, Front. Plant Sci., 7, https://doi.org/10.3389/fpls.2016.00657, 2016.

Xue, B., A, Y., Wang, G., Helman, D., Sun, G., Tao, S., Liu, T., Yan, D., Zhao, T., Zhang, H., Chen, L., Sun, W., and Xiao, J.: Divergent Hydrological Responses to Forest Expansion in Dry and Wet Basins of China: Implications for Future Afforestation Planning, Water Resources Research, 58, e2021WR031856, https://doi.org/10.1029/2021WR031856, 2022.

Yang, H. and Yang, D.: Derivation of climate elasticity of runoff to assess the effects of climate change on annual runoff: DERIVATION OF CLIMATE ELASTICITY OF RUNOFF, Water Resour. Res., 47, https://doi.org/10.1029/2010WR009287, 2011.

Yang, H. and Yang, D.: Climatic factors influencing changing pan evaporation across China from 1961 to 2001, Journal of Hydrology, 414–415, 184–193, https://doi.org/10.1016/j.jhydrol.2011.10.043, 2012.

Yang, H., Xu, H., Huntingford, C., Ciais, P., and Piao, S.: Strong direct and indirect influences of climate change on water yield confirmed by the Budyko framework, Geography and Sustainability, 2, 281–287, https://doi.org/10.1016/j.geosus.2021.11.001, 2021.

Yang, L., Zhao, G., Tian, P., Mu, X., Tian, X., Feng, J., and Bai, Y.: Runoff changes in the major river basins of China and their responses to potential driving forces, Journal of Hydrology, 607, 127536, https://doi.org/10.1016/j.jhydrol.2022.127536, 2022.

Yang, Y., Xiao, P., Feng, X., and Li, H.: Accuracy assessment of seven global land cover datasets over China, ISPRS Journal of Photogrammetry and Remote Sensing, 125, 156–173, https://doi.org/10.1016/j.isprsjprs.2017.01.016, 2017.

Yang, Y., Roderick, M. L., Zhang, S., McVicar, T. R., and Donohue, R. J.: Hydrologic implications of vegetation response to elevated CO2 in climate projections, Nature Clim Change, 9, 44–48, https://doi.org/10.1038/s41558-018-0361-0, 2019.

Zeng, F., Ma, M.-G., Di, D.-R., and Shi, W.-Y.: Separating the Impacts of Climate Change and Human Activities on Runoff: A Review of Method and Application, Water, 12, 2201, https://doi.org/10.3390/w12082201, 2020.

Zhai, R. and Tao, F.: Climate Change in China Affects Runoff and Terrestrial Ecosystem Water Retention More Than Changes in Leaf Area Index and Land Use/Cover Over the Period 1982–2015, JGR Biogeosciences, 126, e2020JG005902, https://doi.org/10.1029/2020JG005902, 2021.

Zhang, B., Tian, L., Zhao, X., and Wu, P.: Feedbacks between vegetation restoration and local precipitation over the Loess Plateau in China, Sci. China Earth Sci., 64, 920–931, https://doi.org/10.1007/s11430-020-9751-8, 2021a.

Zhang C., WU C., KUAI S., PENG Z., Chang R., and ZHANG S.: Water-heat coupling model-based study on runoff driving mechanism of Zhenjiangguan Watershed, Water Resources and Hydropower Engineering, 53, 78–87, https://doi.org/10.13928/j.cnki.wrahe.2022.08.008, 2022a.

Zhang, J., Zhang, Y., Sun, G., Song, C., Dannenberg, M. P., Li, J., Liu, N., Zhang, K., Zhang, Q., and Hao, L.: Vegetation greening weakened the capacity of water supply to China's South-to-North Water Diversion Project, Hydrol. Earth Syst. Sci., 25, 5623–5640, https://doi.org/10.5194/hess-25-5623-2021, 2021b.

Zhang, J., Zhang, Y., Sun, G., Song, C., Li, J., Hao, L., and Liu, N.: Climate Variability Masked Greening Effects on Water Yield in the Yangtze River Basin During 2001–2018, Water Resources Research, 58, e2021WR030382, https://doi.org/10.1029/2021WR030382, 2022b.

Zhang, S., Yang, H., Yang, D., and Jayawardena, A. W.: Quantifying the effect of vegetation change on the regional water balance within the Budyko framework, Geophysical Research Letters, 43, 1140–1148, https://doi.org/10.1002/2015GL066952, 2016a.

Zhang, X., Zhao, T., Xu, H., Liu, W., Wang, J., Chen, X., and Liu, L.: GLC_FCS30D: the first global 30 m land-cover dynamics monitoring product with a fine classification system for the period from 1985 to 2022 generated using dense-time-series Landsat imagery and the continuous change-detection method, Earth Syst. Sci. Data, 16, 1353–1381, https://doi.org/10.5194/essd-16-1353-2024, 2024.

Zhang, Y., Song, C., Sun, G., Band, L. E., McNulty, S., Noormets, A., Zhang, Q., and Zhang, Z.: Development of a coupled carbon and water model for estimating global gross primary productivity and evapotranspiration based on eddy flux and remote sensing data, Agricultural and Forest Meteorology, 223, 116–131, https://doi.org/10.1016/j.agrformet.2016.04.003, 2016b.

Zhao, F., Wu, Y., Ma, S., Lei, X., and Liao, W.: Increased Water Use Efficiency in China and Its Drivers During 2000–2016, Ecosystems, 25, 1476–1492, https://doi.org/10.1007/s10021-021-00727-4, 2022.

Zhou, S., Yu, B., Huang, Y., and Wang, G.: The effect of vapor pressure deficit on water use efficiency at the subdaily time scale, Geophysical Research Letters, 41, 5005–5013, https://doi.org/10.1002/2014GL060741, 2014.

Zhou, S., Yu, B., Lintner, B. R., Findell, K. L., and Zhang, Y.: Projected increase in global runoff dominated by land surface changes, Nat. Clim. Chang., 13, 442–449, https://doi.org/10.1038/s41558-023-01659-8, 2023.